LETTERS

Aerodynamics of the hovering hummingbird

Douglas R. Warrick[1], Bret W. Tobalske[2] & Donald R. Powers[3]

Despite profound musculoskeletal differences, hummingbirds (Trochilidae) are widely thought to employ aerodynamic mechanisms similar to those used by insects. The kinematic symmetry of the hummingbird upstroke and downstroke[1–3] has led to the assumption that these halves of the wingbeat cycle contribute equally to weight support during hovering, as exhibited by insects of similar size[4]. This assumption has been applied, either explicitly or implicitly, in widely used aerodynamic models[1,5–7] and in a variety of empirical tests[8,9]. Here we provide measurements of the wake of hovering rufous hummingbirds (*Selasphorus rufus*) obtained with digital particle image velocimetry that show force asymmetry: hummingbirds produce 75% of their weight support during the downstroke and only 25% during the upstroke. Some of this asymmetry is probably due to inversion of their cambered wings during upstroke. The wake of hummingbird wings also reveals evidence of leading-edge vortices created during the downstroke, indicating that they may operate at Reynolds numbers sufficiently low to exploit a key mechanism typical of insect hovering[10,11]. Hummingbird hovering approaches that of insects, yet remains distinct because of effects resulting from an inherently dissimilar—avian—body plan.

The convergence of hummingbirds and nectivorous insects in the form and use of wings is a testament to the strength of the selective forces imposed: the demands of a high-energy flux way of life, and of locomotion in a fluid medium. The strong similarities in morphology and kinematics—and hence in Reynolds (Re) numbers—have led to the prediction that, during hovering flight in particular, hummingbirds and insects produce lift by using similar aerodynamic mechanisms[1,3,12,13]. Studies of the flight of hawkmoths (Re ≈ 8000) suggest twofold similarities: the use of symmetrical hovering, where the upstroke and downstroke contribute roughly equally to weight support; and the use of aerodynamic mechanisms previously unrecognized in birds, including dynamic stall and leading-edge vortices, to augment lift[10,11,14–16]. The purpose of the present study was to test, with the use of digital particle imaging velocimetry (DPIV), whether hummingbirds have completely converged with insects in terms of the aerodynamic contributions of the upstroke and downstroke, and to examine the wake structure for evidence that hummingbirds exploit low-Re aerodynamic mechanisms characteristic of insect flight.

We sampled the wake produced by rufous hummingbirds (*Selasphorus rufus*, $n = 3$; Re during hover ≈ 3,000, average wing chord as characteristic length) as they hovered in the $60 \times 60 \times 85 \, cm^3$ test section of an idle wind tunnel with the bottom removed. The wake structure was measured less than four wing chord lengths (4 cm) below the wings, 8–14 ms after the kinematic events that produced it, and before the wake structure significantly degraded owing to viscosity or near-field interaction with the still-active wings[17]. The birds were trained to fly to a feeder (a 1-ml syringe containing a 20% sucrose solution), the placement of which was manipulated to allow two-dimensional sampling of different

portions of the wake from up to three chord lengths (3 cm) above the bird to eight chord lengths (8 cm) below the bird. Simultaneous digital video (500 frames s^{-1}), taken from directly above the bird, allowed the synchronization of DPIV images with wing kinematics. The wake was sampled in five frontal (Fig. 1a, b) and parasagittal planes (Fig. 1c, d) taken at 1-cm intervals.

Frontal-plane samples of the wake revealed trailing-tip vortices as the wings passed in and out of the plane of the laser sheet (Fig. 1b); parasagittal planes revealed the structure of the starting and stopping vortices of the downstroke, the starting vortices of the upstroke, and any leading-edge vorticity (LEV) shed at the end of the halfstroke[10] (Fig. 1d). For both sampling planes, only images taken during the transition from upstroke to downstroke revealed distinct structure created by the immediately previous upstroke and downstroke, respectively. At all other periods in the wingbeat cycle, the dominant momentum jet produced by the downstroke annihilated any major vortex structures produced by the upstroke. Sixty-five images were
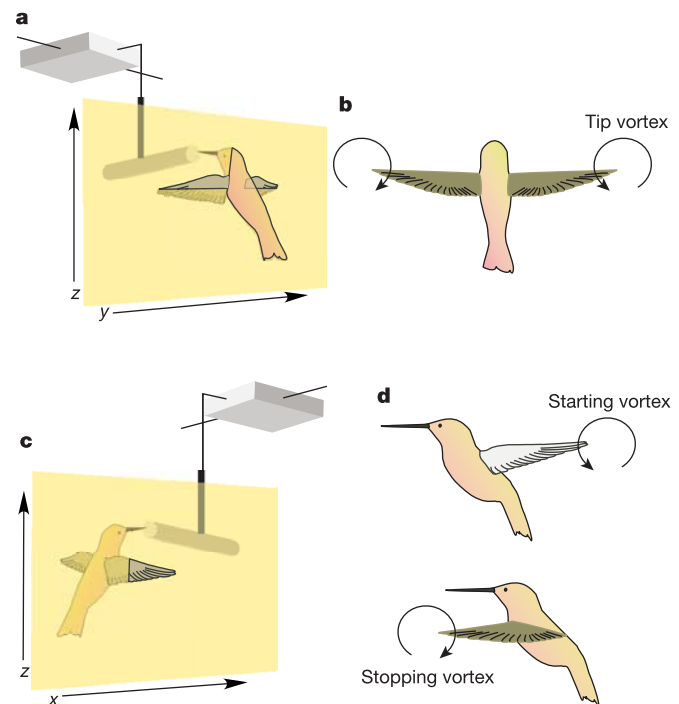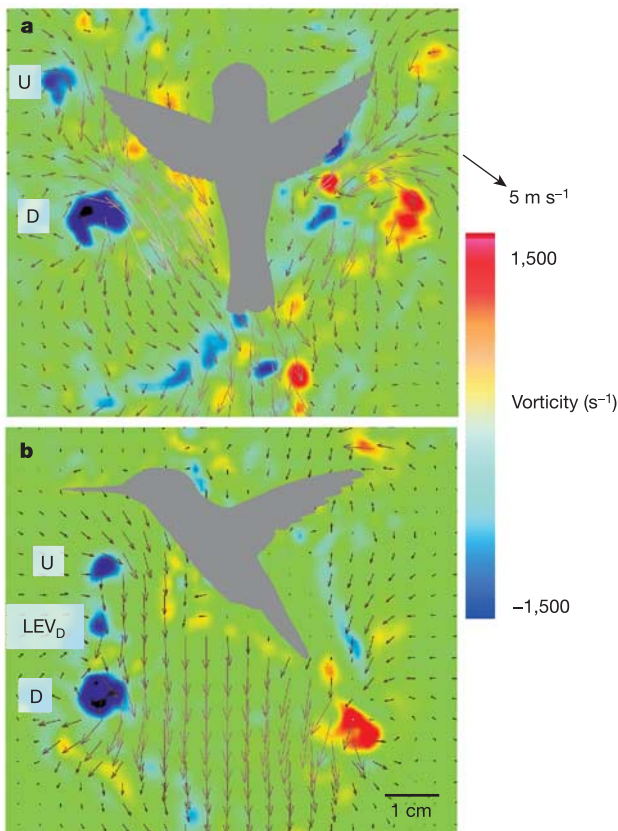

Figure 1 | DPIV methodology. a, Birds hovering at a feeder positioned such that the two-dimensional laser light sheet illuminated wake-entrained oil particles moving in a frontal plane. **b**, The expected wake structures within the frontal plane[5,6]. **c**, Light sheet oriented in the parasagittal plane, centred at midwing. **d**, The expected wake structures within the parasagittal plane[5,6].

[1]Department of Zoology, Oregon State University, 3029 Cordley Hall, Corvallis, Oregon 97331, USA. [2]Department of Biology, University of Portland, 5000 North Willamette Boulevard, Portland, Oregon 97203, USA. [3]Biology Department, George Fox University, 414 North Meridian Street, Newberg, Oregon 97132, USA.

analysed for the aerodynamic contribution of the two halves of the wingbeat cycle, and paired comparisons of the upstroke and downstroke tip vortices (frontal planes; Fig. 2a) and downstroke stopping and upstroke starting vortices (parasagittal planes (Fig. 2b) were made.
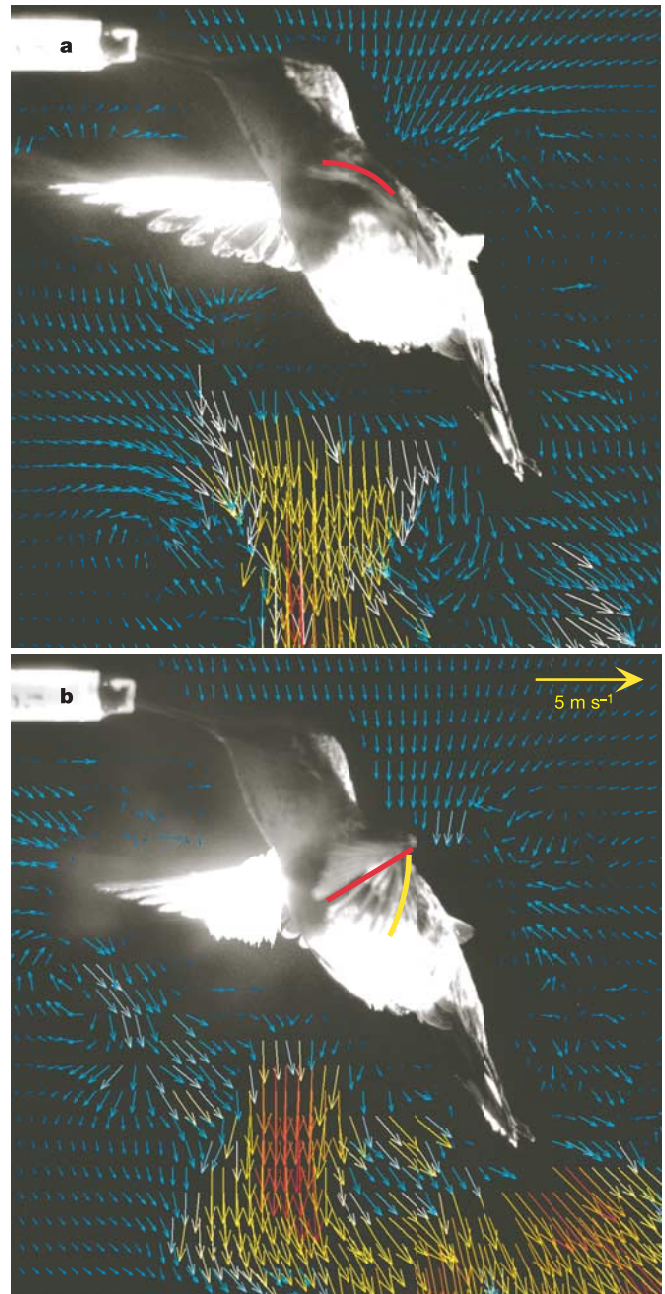
Consistent with their steady position in hovering was the observation that there was sufficient circulation, Γ, in the tip vortices, and adequate separation between vortex cores, to support the body weight of the hummingbirds. The circulation (mean ± s.d.) relative to that required for weight support was 111 ± 20% for bird 1 ($n = 11$), 94 ± 17% for bird 2 ($n = 25$) and 103 ± 20% for bird 3 ($n = 29$); the range for all samples was 57–147% ($n = 65$).

Eight of 15 parasagittal samples revealed wake structures consistent with the production of leading-edge vortices during the downstroke. In these samples, at the transition from downstroke to upstroke, two cores of vorticity, both rotating in the same direction, were shed in quick succession. The first (LEV_D; Fig. 2b) is consistent with the shedding of a leading-edge vortex generated by the previous downstroke. As demonstrated by robotic models operating at similar Re (ref. 10), this vortex can remain attached to the wing beneath the bound circulation and is shed during the supinating rotation at the beginning of upstroke. Soon afterwards, the starting vortex of the upstroke is produced (U, Fig. 2b).

Given the strength of this presumptive leading-edge vortex, and if we assume that it was feeding into the tip vortex strength[10] (as measured in the frontal samples), the leading-edge vortex provided 15 ± 4% of the circulation of the tip vortex wake during downstroke. Because leading-edge vortices can be generated during the rapid ventral rotation (pronation) of the wing—before the downstroke, wing movement can generate a more traditional bound vortex—it is possible that a more important function of the formation of the leading-edge vortex is to draw air downwards during wing turn-around[13], filling the gap in aerodynamic force production at wing

Figure 2 | Flow field vorticity. a, Single-field sample of a hummingbird wake taken at the end of the upstroke, in frontal view with the interrogation plane through the shoulder, revealing the tip vortices of downstroke D and upstroke U. b, Single-field sample of a hummingbird wake at the end of the upstroke, in parasagittal plane with the interrogation plane passing through the midwing during the middle of each half wingbeat (about 3 cm from the midline of the bird's body). Between the downstroke stopping vortex D and the upstroke starting vortex U is a pocket of vorticity LEV_D presumably created at the leading edge of the wing during the rapid wing pronation at the beginning of the preceding downstroke, and carried through the downstroke to be shed during the supination at the beginning of the upstroke.

Figure 3 | Hummingbird wing presentation and flow field. a, The profile of the hummingbird wing during mid-downstroke. A red line is drawn just above the dorsal surface of the wing to highlight the camber, typical of a bird wing. b, The proximal part of the wing, to the left of the yellow line, is not as supinated (inverted) as the distal portion, to the left of the red line. The presentation of these two portions of the wing is typical for an avian upstroke, and results in an airfoil of reduced efficacy relative to wing downstroke. Vector scale top right.

turnaround, and perhaps facilitating the rapid development of more typical bound circulation.

Pairwise comparisons of upstroke and downstroke circulation within a wingbeat cycle revealed that the downstroke provides the vast majority of the weight support during hovering (averages for individuals, 74 ± 7%, 77 ± 5% and 76 ± 6%; paired *t*-test for differences in circulation between upstroke/downstroke vortex pairs, $P < 0.0001$). Downstroke circulation varied less than that of the upstroke (coefficient of variation for all birds, all samples: 0.21 versus 0.27).

Long-standing kinematic data have suggested that hummingbird upstroke and downstroke are essentially symmetrical[1–3]. Our own three-dimensional kinematics indicate that wing span is indeed fairly symmetrical (upstroke 91 ± 4 mm; downstroke 93 ± 3 mm). The angular velocity of the wing is slightly less during the upstroke ($146 ± 15$ rad s^{-1}) than during the downstroke ($196 ± 26$ rad s^{-1}). Observed differences in area (S) and velocity (v) applied to a general lift (L) formula ($L \propto v^2 S C_L$) suggest that the downstroke should produce 64% of weight support.

The remaining variable, lift coefficient (C_L), is a function of angle of attack. On average, the angle of attack (measured at midwing, halfway between the wrist and tip) at mid-downstroke is greater than during mid-upstroke ($36 ± 12°$ versus $26 ± 13°$), the higher angles during downstroke allowed by the positive camber typical of bird wings (Fig. 3a). Lift coefficients vary linearly with angle of attack; adding this difference in C_L would result in a downstroke that produced about 70% of weight support—somewhat less than the 75% value observed in the wake. The remainder of the disparity might be produced by more subtle asymmetries—in particular, the angle of attack and performance of the proximal wing, which does not seem to reverse camber during the upstroke (Fig. 3b). In addition, we saw no evidence of leading-edge vorticity either developing at the beginning of the upstroke or being shed at the end of it.

Although the wing kinematics of hummingbirds shows strong convergence with that of certain insects (for example the hawkmoth, *Manduca sexta*), there are fundamental musculoskeletal and plan-form material properties that limit their ability to produce the wingbeat cycle symmetry found in these insects. In comparison with other birds, the hummingbird shoulder joint allows greater rotation about the long axis of the humerus, and the relatively long primaries of hummingbirds allows much more of the wing planform to be inverted during the upstroke[2,3,18]. Nonetheless, our results show that the efficacy of the hummingbird wing at negative angles of attack in the upstroke compares poorly with its performance at positive angles of attack during the downstroke. Although camber in the distal wing could conceivably be reversed, in the proximal wing thin feathers trailing behind thick musculoskeletal elements create camber that is not reversed during the upstroke (Fig. 3b). In contrast, the elastic qualities of insect wings in response to both aerodynamic[19] and inertial forces[20] allow them to reverse their camber fully, and therefore to develop high lift coefficients during both half-strokes[15].

Hummingbirds and insects have evolved for sustained hovering flight from vastly different ancestral directions, and their distinct phylogenies underlie the differences in their aerodynamic styles. In all other birds—and, presumably, hummingbird ancestors—the downstroke provides 100% of weight support during slow flight and hovering[7]. Given that many birds possess the mass-specific power (using anaerobic metabolism) to hover for short periods, the selective pressure on hummingbird ancestors was probably for increased efficiency[1,8] (resulting in stiff wings with greatly simplified kinematics), and an upstroke muscle (the supracoracoideus) that makes the recovery stroke rapid, while contributing enough to the hovering power requirements to allow the downstroke muscle (the pectoralis) to operate within its aerobic limits. In other words, this pseudosymmetrical wingbeat cycle is good enough, and although

hummingbirds do not exhibit the elegant aerodynamic symmetry of insects, natural selection rewards 'good enough' as richly as it does our aesthetic ideals.

METHODS

DPIV. Our DPIV system was manufactured by LaVision Inc.; recording and analysis were accomplished with DaVis (v6.0.2). We used a dual-cavity pulsed 50-mJ Nd:YAG laser to illuminate a flow field about 3 mm thick, with planar dimensions spanning the wake of the hummingbird from three chord lengths above to eight chord lengths below the wing root. The air was seeded with submicrometre-sized particles of olive oil vapour, generated with a Laskin nozzle at a rate of $7 × 10^{10}$ particles s^{-1}. Particle illumination was recorded with a 1,376-pixel × 1,040-pixel charge-coupled device camera. To calculate velocity, a cross-correlation with adaptive multipass was employed; this method correlates within areas beginning at 64 pixels × 64 pixels and decreasing to 16 pixels × 16 pixels with 50% overlap. A correlation peak error of 0.1 pixel, and an average particle separation in the wake of 12 pixels, produced 1% error[21,22]; combined with optical distortion and particle-fluid fidelity error[22], our observed measurement error was 2.3 ± 0.5%. To compute vorticity (ω, s^{-1}), we post-processed vector fields with a median filter and then computed rot$z$(dy/dx). Background ω, measured 2–3 cm outside the wake structure, was less than 2% of peak ω in the wake; a 10% mask was applied to eliminate this background noise and allow the definition of wake structures. The scaled pixel area of the remaining wake structure was then summed, yielding total circulation.

Circulation and weight support. We measured circulation (Γ, m^2 s^{-1}) in the trailing-tip vortices by integrating ω with respect to area (m^2). We limited our analysis to views where vortex cores were normal to the sampling plane (parasagittal, centred at midwing; frontal, centred at wing root)[23]. We tested whether observed Γ was sufficient to support body weight by comparing observed Γ with circulation required (Γ_o), where $\Gamma_o = WT/\rho S$, where W is body weight (N), T is time per wingbeat (s) and S is the projected horizontal area swept by the two wings (m^2) (ref. 23).

Kinematics. Separate flight trials ($n = 4$ birds) were recorded with two synchronized high-speed digital video cameras operating at 500 Hz sampling and a shutter speed of 1/1,000 s. We merged two-dimensional coordinates from each camera into a single three-dimensional coordinate space by using the direct linear transformation coefficients derived from a 16-point calibration frame[24]. From these data we calculated the horizontal projection of the stroke plane, the angular velocity of the wing (rad s^{-1}) and the angle of attack of the midwing (degrees) relative to the incurrent air flow. Incurrent air velocity was the sum of translational velocity of the wing and average three-dimensional air velocity computed with DPIV data from the frontal and sagittal planes, which is dominated by a mean downward velocity of 1.1 m s^{-1}.

1. Weis-Fogh, T. Energetics of hovering flight in hummingbirds and in *Drosophila*. *J. Exp. Biol.* **56**, 79–104 (1972).
2. Stolpe, V. M. & Zimmer, K. Der Schwirrflug des Kolibri im Zeitlupenfilm. *J. Ornithol.* **87**, 136–155 (1939).
3. Greenwalt, C. H. The wings of insects and birds as mechanical oscillators. *Proc. Am. Phil. Soc.* **104**, 605–611 (1960).
4. Wilmott, A. P. & Ellington, C. P. The mechanics of flight in the hawkmoth *Manduca sexta*. II. Aerodynamic consequences of kinematic and morphological variation. *J. Exp. Biol.* **200**, 2723–2745 (1997).
5. Rayner, J. M. V. A vortex theory of animal flight. I. The vortex wake of a hovering animal. *J. Fluid Mech.* **91**, 697–730 (1979).
6. Ellington, C. P. The aerodynamics of hovering insect flight. V. A vortex theory. *Phil. Trans. R. Soc. Lond. B* **305**, 79–113 (1984).
7. Norberg, U. M. *Vertebrate Flight: Mechanics, Physiology, Morphology, Ecology, and Evolution* (Springer, Berlin, 1990).
8. Wells, D. Muscle performance in hovering hummingbirds. *J. Exp. Biol.* **78**, 39–57 (1993).
9. Tobalske, B. W., Altshuler, D. L. & Powers, D. R. Take-off mechanics in hummingbirds (Trochilidae). *J. Exp. Biol.* **207**, 1345–1352 (2004).
10. van den Berg, C. & Ellington, C. P. The vortex wake of a 'hovering' model hawkmoth. *Phil. Trans. R. Soc. Lond. B* **352**, 329–340 (1997).
11. Dickinson, M. H., Lehmann, F. & Sane, S. P. Wing rotation and the aerodynamic basis of insect flight. *Science* **284**, 1954–1960 (1999).
12. Dudley, R. *The Biomechanics of Insect Flight* (Princeton Univ. Press, Princeton, 2000).
13. Altshuler, D., Dudley, R. & Ellington, C. P. Aerodynamic forces of revolving hummingbird wings and wing models. *J. Zool. (Lond.)* **264**, 327–332 (2004).
14. Willmott, A. P. & Ellington, C. P. The mechanics of flight in the hawkmoth *Manduca sexta*. I. Kinematics of hovering and forward flight. *J. Exp. Biol.* **200**, 2705–2722 (1997).

15. Willmott, A. P., Ellington, C. P. & Thomas, A. L. R. Flow visualization and unsteady aerodynamics in the flight of the hawkmoth *Manduca sexta*. *Phil. Trans. R. Soc. Lond. B* **352,** 303–316 (1997).

16. Usherwood, J. R. & Ellington, C. P. The aerodynamics of revolving wings. I. Model hawkmoth wings. *J. Exp. Biol.* **205,** 1547–1564 (2002).

17. Tytell, E. D. & Ellington, C. P. How to perform measurements in a hovering animal's wake: physical modelling of the vortex wake of the hawkmoth, *Manduca sexta*. *Phil. Trans. R. Soc. Lond. B* **358,** 1559–1566 (2003).

18. Tobalske, B. W., Hedrick, T. L. & Biewener, A. A. Wing kinematics of avian flight across speeds. *J. Avian Biol.* **34,** 177–184 (2003).

19. Wootten, R. J. Geometry and mechanics of insect hindwing fans: a modelling approach. *Proc. R. Soc. Lond. B* **262,** 181–187 (1995).

20. Combes, S. A. & Daniel, T. L. Into thin air: contributions of aerodynamic and inertial-elastic forces to wing bending in the hawkmoth *Manduca sexta*. *J. Exp. Biol.* **206,** 2999–3006 (2003).

21. Spedding, G. R., Hendenstrom, A. & Rosen, M. Quantitative studies of the wakes of freely flying birds in a low-turbulence wind tunnel. *Exp. Fluids* **34,** 291–303 (2003).

22. Raffel, M., Willert, C. & Kompenhans, J. *Particle Image Velocimetry: A Practical Guide* (Springer, Berlin, 2000).

23. Spedding, G. R., Rosen, M. & Hedenstrom, A. A family of vortex wakes generated by a thrush in free flight in a wind tunnel of its entire natural range of flight speeds. *J. Exp. Biol.* **206,** 2313–2344 (2003).

24. Hedrick, T. L., Tobalske, B. W. & Biewener, A. A. Estimates of gait change based on a three-dimensinal analysis of flight in cockatiels (*Nymphicus hollandicus*) and ringed turtle doves (*Stretopelia risoria*). *J. Exp. Biol.* **205,** 1389–1409 (2002).